Spin-orbit coupling controlled two-dimensional magnetism in chromium trihalides

Inhee Lee [1,*] Jiefu Cen [2] Oleksandr Molchanov [1] Shi Feng [1] Warren L. Huey,[3] Johan van Tol [4] Joshua E. Goldberger [3] Nandini Trivedi,[1] Hae-Young Kee,[2,5] and P. Chris Hammel [1,†]

[1]*Department of Physics, The Ohio State University, Columbus, Ohio 43210, USA*

[2]*Department of Physics, University of Toronto, Toronto, Ontario, Canada M5S 1A7*

[3]*Department of Chemistry and Biochemistry, The Ohio State University, Columbus, Ohio 43210, USA*

[4]*National High Magnetic Field Laboratory, Florida State University, Tallahassee, Florida 32310, USA*

[5]*Canadian Institute for Advanced Research, CIFAR Program in Quantum Materials, Toronto, Ontario, Canada M5S 1M1*

(Received 17 July 2024; revised 4 December 2025; accepted 8 December 2025; published 5 January 2026)

CrX_3 (X = Cl, Br, I) have the same crystal structure and Hamiltonian but different ligand spin-orbit coupling (SOC) constant λ_X, providing an excellent material platform exploring for exotic two-dimensional (2D) spin orders. Their microscopic mechanism underlying 2D spin physics remain unestablished, along with experimental corroboration of Kitaev exchange interaction, central to realizing topological quantum spin liquids. Finding direct evidence for Kitaev interaction and determining its value has been an essential but formidable challenge in Kitaev physics. Here we report the direct Kitaev interaction signature in magnetic anisotropy measured by ferromagnetic resonance (FMR) spectroscopy. We present measured values of Heisenberg J, Kitaev K, and off-diagonal symmetric Γ exchange interactions in CrX_3 determined using FMR and exact diagonalization. K and Γ exhibit dominant dependencies on λ_X, indicating its central role in 2D magnetism. Our study provides a foundation for designing 2D magnetic materials exhibiting novel behaviors by tuning intrinsic material parameters such as SOC.

DOI: 10.1103/qg64-ztxj

Since the discovery of CrI_3 atomic monolayer ferromagnets [1], two-dimensional (2D) van der Waals (vdW) magnets have attracted much attention due to their potential for hosting exotic 2D quantum spin physics such as bosonic topologically protected chiral edge states [2–5], Kitaev quantum spin liquids [6–9] and skyrmions [10], as well as developing 2D spintronics devices integrated with other vdW materials such as transition metal dichalcogenides and graphene [11,12]. The Kitaev interaction, which must exist in the chromium trihalide family (CrX_3, X = Cl, Br, I) due to its crystal symmetry [8,13,14], is the core element in realizing topological quantum spin liquid states. While there are experimental reports of half-quantized thermal Hall conductance [15,16] and signatures of propagating Majorana fermions in α-$RuCl_3$, there are also counterproposals [17,18], leaving its existence under debate and ambiguity as to both its estimated value and sign. Moreover, while previously observed magnetic behaviors associated with quantum spin liquids have been interpreted based on the Kitaev model, there is little direct evidence of their relevance to Kitaev interaction.

The large spin-wave gap at the Dirac point observed in CrI_3 by inelastic neutron scattering (INS) [3] has been considered a possible experimental signature of the Kitaev interaction [8], but this is controversial, as the next-nearest-neighbor (NNN) Dzyaloshinskii-Moriya (DM) [3,19] interaction could also open this gap. In any case, the Kitaev and NNN DM interactions require unreasonably large values to account for the large Dirac gap. It has furthermore been pointed out that the measured gap size is very sensitive to INS experimental conditions such as sample mosaic, resolution, and momentum integration range leading to the possibility that gap size can be significantly overestimated, especially at the Dirac point where spin waves rapidly disperse [5,20]. Indeed, two independent INS studies recently reported conflicting values for the size of the Dirac gap in $CrBr_3$: 3.5 meV [21] in one case versus no gap in another [22]. The Dirac gap size of CrI_3 was adjusted from 5 to 2.8 meV through improved INS measurements [5]. This situation calls for a complementary approach to obtaining a reliable value of the Kitaev interaction.

Ferromagnetic resonance (FMR) is a high-resolution ($\sim\mu$eV) spectroscopic tool that enables determination of the Kitaev interaction through accurate measurement of the interaction of the collection of ordered spins with both internal and external environments. Similar magnetic resonance techniques have been applied to spin excitations associated with fractionalized Majorana excitations in α-$RuCl_3$ [23,24]. The first FMR study of CrI_3 described the global coherent spin dynamics of the sample in magnetic resonance by applying mean-field theory to the Hamiltonian, converting the multispin interaction problem into a single spin problem [8].

*Contact author: lee.2338@osu.edu

†Contact author: hammel@physics.osu.edu

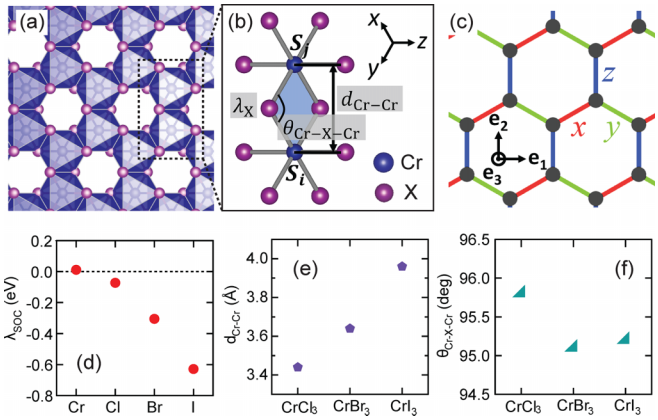

FIG. 1. (a) 2D crystal structure of CrX_3 monolayer. (b) The parameters regarding the superexchange interaction via X^- ligand ions between two Cr^{3+} ion spins of $\mathbf{S_i}$ and $\mathbf{S_j}$ in the neighboring octahedra along a z bond: ligand SOC constant λ_X, Cr–X–Cr bond angle $\theta_{Cr-X-Cr}$, and Cr–Cr distance d_{Cr-Cr}. (c) 2D honeycomb lattice spin model having x-, y-, and z-bond-dependent spin interactions. (d) The spin-orbit coupling constant λ_{SOC} of the atomic orbital obtained from atomic optical spectroscopy [28–30]. (e) Cr–Cr distance d_{Cr-Cr} [31]. (f) Cr–X–Cr bond angle $\theta_{Cr-X-Cr}$ [32].

However, this approximation removes all the anisotropic components of the Kitaev interaction, rendering it isotropic and thus indistinguishable from Heisenberg exchange. Recent theoretical studies based on symmetry analysis showed that the Kitaev interaction leads to anisotropy in the magnetic response between $\mathbf{e_1}$ and $\mathbf{e_2}$ directions. Kitaev interaction also leads to an anisotropy of the FMR frequency, depending on the orientation of the magnetic field within the $\mathbf{e_1}$–$\mathbf{e_3}$ plane as indicated in Fig. 1(c) [13,14].

The CrX_3 materials have the same crystal structure and are described by the same Hamiltonian as A_2IrO_3 (A = Na, Li) [25,26] and α-$RuCl_3$ [6], known potential honeycomb Kitaev materials, but CrX_3 has contrasting features. For A_2IrO_3 and α-$RuCl_3$, the transition metal ion has effective spin-1/2 and dominant SOC, $\lambda_M \mathbf{L}\cdot\mathbf{S}$ where λ_M plays an essential role in determining exchange interactions. On the other hand, CrX_3 has spin-3/2, and λ_X, the SOC of the p orbital of ligand atom X, is considered to be the main source of superexchange interactions. In this regard, a theoretical microscopic analysis of CrX_3 was recently performed to find the origin of spin interactions and showed that indeed Kitaev interaction can arise for 3/2-spin by the ligand SOC [27].

CrX_3 (X = Cl, Br, I) share a common crystal structure and a common Hamiltonian but have different λ_X. Therefore, λ_X is the key single parameter that can characterize this well-defined 2D magnetic platform once its relationship with Hamiltonian's spin interaction constants is clearly established. Nevertheless, there has been no systematic experimental study to elucidate this.

Here we present the measured spin interaction constants for three CrX_3 compounds determined using field-angle-dependent FMR spectroscopy and exact diagonalization (ED). Furthermore, we investigate the relationship between those values and the ligand SOC λ_X. The magnetic anisotropy distinctively originating from the Kitaev interaction appears in FMR spectra as a unique experimental signature that is strongly dependent on λ_X. Unlike mean-field theory, ED directly incorporates bond-dependent spin-spin interactions for multiple spins, allowing us to determine the Kitaev interaction for CrX_3 from these experimental data.

CrX_3 spin systems can be described with a 2D honeycomb lattice spin model which has bond-dependent anisotropic exchange interactions [see Fig. 1(c)]. CrX_3 have the edge-sharing octahedral 2D crystal structure in Fig. 1(a), and their spin model is based on the anisotropic superexchange interactions between two Cr spins via Cr–X–Cr bonds arising from the SOC of ligand X [see Fig. 1(b)]. Based on the crystal symmetries, the Hamiltonian is

$$\mathcal{H} = \mathcal{H}_E + \mathcal{H}_D + \mathcal{H}_Z, \tag{1}$$

where

$$\mathcal{H}_E = \sum_{\langle ij\rangle\in\lambda\mu(\nu)} \left[J\mathbf{S}_i\cdot\mathbf{S}_j + KS_i^\nu S_j^\nu + \Gamma(S_i^\lambda S_j^\mu + S_i^\mu S_j^\lambda)\right] \tag{2}$$

describes exchange interactions,

$$\mathcal{H}_D = \sum_{i>j} \frac{g^2\mu_B^2}{r_{ij}^3}\left[\mathbf{S}_i\cdot\mathbf{S}_j - \frac{3}{r_{ij}^2}(\mathbf{S}_i\cdot\mathbf{r_{ij}})(\mathbf{S}_j\cdot\mathbf{r_{ij}})\right] \tag{3}$$

describes dipole-dipole interactions, and

$$\mathcal{H}_Z = -g\mu_B\mathbf{H}_0\cdot\sum_i \mathbf{S}_i \tag{4}$$

describes Zeeman interactions. $\mathbf{S_i}$ is the spin-3/2 operator for the Cr^{3+} ion at site i. $\langle ij\rangle\in\lambda\mu(\nu)$ denotes that the Cr^{3+} ions at the neighboring sites i, j are interacting via a ν bond, where $\lambda, \mu, \nu \in \{x, y, z\}$. g is the g factor of Cr^{3+}, μ_B is the Bohr magneton, and $\mathbf{r_{ij}}$ is the distance vector joining spins at site i and j. The magnetic anisotropy of CrX_3 is contributed by $\mathcal{H}_E$ and $\mathcal{H}_D$ as magnetocrystalline and shape anisotropy, respectively.

We determine J, K, and Γ values from the magnetic anisotropies of CrX_3 measured from the dependencies of their FMR spectra on the magnetic field direction using a sub-THz heterodyne quasioptical electron-spin-resonance spectrometer [33]. FMR spectra are obtained at various θ_H, the angle between the applied magnetic field $\mathbf{H_0}$ and $\mathbf{e_3}$, in the $\mathbf{e_1}$–$\mathbf{e_3}$ plane [see Fig. 2(c) inset]. The applied electromagnetic excitation frequency is $\omega/2\pi = 240$ GHz. Figures 2(a)–2(c) show the evolution of the FMR signal of CrX_3 as a function of H_0 for a series of orientations (θ_H). We obtain the resonance field H_{res} from Lorentzian fits to these spectra. The evolution of $H_{res}(\theta_H)$ for CrX_3 is presented in Figs. 2(d), 2(f), and 2(h). The salient features of this anisotropic behavior is best seen by considering two quantities: $H_U(\theta_H) = H_{res}(\theta_H) - \omega/\gamma$ and $\Delta H_K(\theta_H) = H_{res}(180^\circ - \theta_H) - H_{res}(\theta_H)$ [see Fig. 2(c)].

H_U reveals the uniaxial magnetic anisotropy along $\mathbf{e_3}$ arising from the combination of the Γ interaction in Eq. (2) and the dipole-dipole interaction (shape anisotropy) in Eq. (3). FMR directly measures the magnitude and polarity of the uniaxial magnetic anisotropy given by $\Delta H_U = H_{res}(90^\circ) - H_{res}(0^\circ)$: -5 kOe for $CrCl_3$, $+5$ kOe for $CrBr_3$, and $+35$ kOe for CrI_3. ΔH_U is negative for $CrCl_3$ but positive for $CrBr_3$ and CrI_3, indicating their opposite polarities.

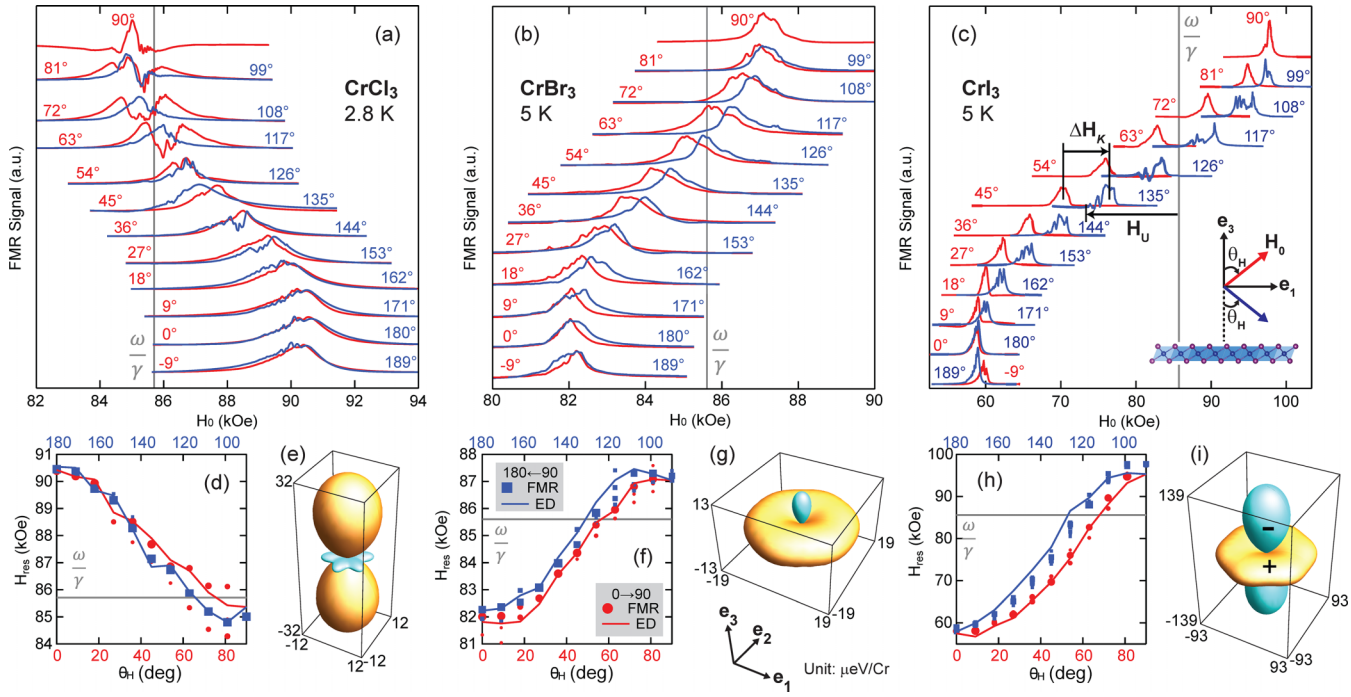

FIG. 2. (a)–(c) FMR spectra of $CrCl_3$, $CrBr_3$, and CrI_3 with varying θ_H describing the orientation of magnetic field $\mathbf{H_0}$ with respect to $\mathbf{e_3}$ in the $\mathbf{e_1}$–$\mathbf{e_3}$ plane [see the inset of (c)]. Each spectrum is offset and scaled moderately for clarity. The gray line labeled $\omega/\gamma = 240$ GHz represents the resonance field H_{res} corresponding to the applied microwave frequency for the free single-ion spin. The shift of H_{res} is characterized by two quantities: $H_U(\theta_H) = H_{res}(\theta_H) - \omega/\gamma$ arising from Γ interaction and dipole-dipole interaction in Eq. (3), and $\Delta H_K(\theta_H) = H_{res}(180^\circ - \theta_H) - H_{res}(\theta_H)$ arising from the asymmetric Kitaev interaction about θ_H and $180^\circ - \theta_H$, indicated by the red and blue arrows, respectively, in the inset of (c). (d) H_{res} vs θ_H extracted from (a) for $CrCl_3$. (e) Total (magnetocrystalline and shape) magnetic anisotropy energy $F(\theta, \phi)$ of $CrCl_3$ as a function of spherical angles θ and ϕ constructed from H_{res} in (d) using Landau theory [8]. (f) H_{res} vs θ_H, and (g) $F(\theta, \phi)$ for $CrBr_3$. (h) H_{res} vs θ_H, and (i) $F(\theta, \phi)$ for CrI_3. In (d), (f), and (h), the symbol size indicates the signal peak area in Lorentzian fits to the FMR spectra and solid lines are exact diagonalization (ED) calculation results. In (e), (g), and (i), orange (cyan) represents positive (negative) values. Panel (c) is adapted from Ref. [8].

ΔH_K is due to the nonuniaxial magnetic anisotropy arising from the asymmetric Kitaev interaction about two symmetric angles θ_H and $180^\circ - \theta_H$, indicated by the red and blue arrows, respectively, in the inset of Fig. 2(c). The sign of ΔH_K inverts at $\theta_H = 0^\circ$ and 180°, such that $H_{res}(9^\circ)$ is lower than $H_{res}(171^\circ)$, but $H_{res}(-9^\circ)$ is higher than $H_{res}(189^\circ)$ [see Figs. 2(b) and 2(c)]. This is consistent with the π rotation symmetry for $\mathbf{e_2}$ of the anisotropic Kitaev interaction [$H_{res}(\theta_H) = H_{res}(\theta_H + 180^\circ) \neq H_{res}(\theta_H - 180^\circ)$] [13]. The magnitude of ΔH_K is minimum for $CrCl_3$, increases in $CrBr_3$, and maximum in CrI_3, corresponding to the increasing strength of λ_X. This is the direct observation of the Kitaev interaction signature in CrX_3 through magnetic anisotropy.

We describe the magnetic anisotropy of CrX_3 measured from FMR as $F(\theta, \phi)$ for two spherical angles θ and ϕ [see Fig. 2(e) for $CrCl_3$, 2(g) for $CrBr_3$, and 2(i) for CrI_3]. These are constructed from $H_{res}(\theta_H)$ using Landau theory, where $F(\theta, \phi)$ is expressed in terms of classical magnetization using mean-field theory and used to calculate the resonant frequency (see Sec. VII of the Supplemental Material [8]). The uniaxial magnetic anisotropy due to magnetocrystalline and shape anisotropy dominates in CrX_3. The $\mathbf{e_3}$ (out-of-plane) axis is the easy axis for $CrBr_3$ and CrI_3, but the hard axis for $CrCl_3$.

We determine the values of J, K, and Γ of the Hamiltonian in Eq. (2) by fitting our FMR data $H_{res}(\theta_H)$ to the values obtained from ED calculations with 12 sites of $S = 3/2$ for 240 GHz [33]. ED provides two sets of values for J, K, and Γ corresponding to $K > 0$ and $K < 0$ for CrX_3. According to a recent microscopic theory for CrX_3 [27], J and K have opposite signs, with $(J > 0, K < 0)$ corresponding to t_{2g}-t_{2g} interaction and $(J < 0, K > 0)$ to e_g–t_{2g} interaction. Since J is negative for both sets we obtain, K must be positive, and e_g–t_{2g} interaction is thought to dominate in these ferromagnetic systems. This further implies that the superexchange processes via p orbitals of ligand X play a crucial role in determining spin interactions.

The values of J, K, and Γ for $K > 0$ in Figs. 3(a)–3(d) and Table I generate values that well match the FMR data for $H_{res}(\theta_H)$ shown in Figs. 2(d), 2(f), and 2(h). Figure 3(a) shows the relative energy scale of these values: $|J| \gg |K| \gg |\Gamma|$ for all three CrX_3 compounds. This is consistent with the

TABLE I. Spin exchange interaction constant values in the Hamiltonian Eq. (2) of CrX_3 determined using FMR and ED.

Coupling Constant	Value (meV) $CrCl_3$	$CrBr_3$	CrI_3
J	−0.69	−1.3	−2.2
K	0.019	0.19	0.92
Γ	−0.0032	−0.021	−0.079

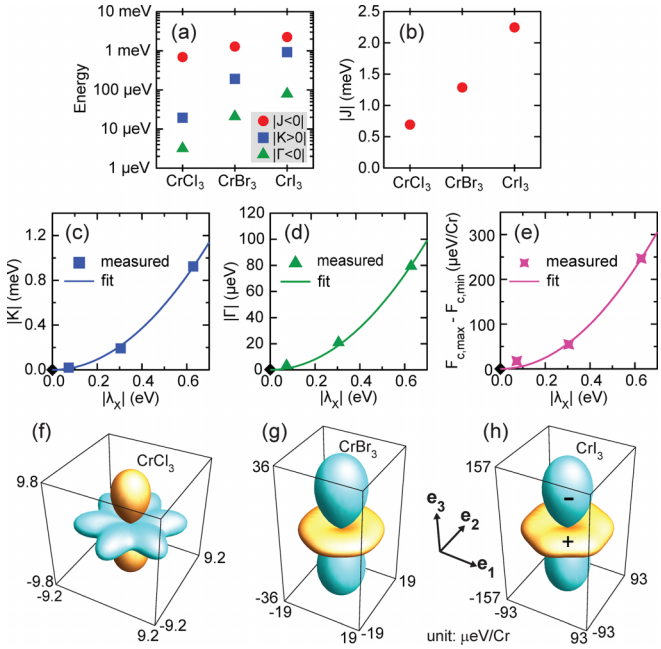

FIG. 3. (a) Comparison of absolute values of Heisenberg J, Kitaev K, and off-diagonal symmetric Γ exchange interactions for CrX_3. (b) $|J|$ values for CrX_3. (c) $|K|$, (d) $|\Gamma|$, and (e) $F_{c,max} - F_{c,min}$ values for three $|\lambda_X|$ values corresponding to CrX_3 in Fig. 1(d) and their quadratic monomial fits (solid lines) based on the theory of [27] with one more data point (black diamond) added, assuming that K, Γ, and $F_{c,max} - F_{c,min}$ become zero when $\lambda_X = 0$. Here F_{max} and F_{min} are the maximum and minimum values of $F_c(\theta, \phi)$ for each CrX_3 in (f)–(h). (f)–(h) Magnetocrystalline anisotropy energy $F_c(\theta, \phi)$ of $CrCl_3$, $CrBr_3$, and CrI_3 obtained after subtracting the shape anisotropy from F in Figs. 2(e), 2(g), and 2(i), respectively. Orange (cyan) represents positive (negative) values.

energy scale of $|J| \gg |K| (\sim r^2|J|) \gg |\Gamma| (\sim 0)$ that emerges from recent microscopic second-order perturbation theory for $S = 3/2$, where $r = \lambda_X/\Delta_{pd}$ and Δ_{pd} is the atomic energy difference between the transition metal and ligand sites [27]. The K and Γ values for CrI_3 here are in reasonable agreement (within 20%) with these exchange constants calculated using density functional theory (DFT) [34].

Next, we determine the universal dependencies of K and Γ in Fig. 3 on the absolute value of the ligand SOC, $|\lambda_X|$. As shown in Fig. 1(d), $|\lambda_X|$ increases in order of increasing ligand mass: Cl, Br, and I. And all are much larger than the Cr $3d$ orbital $|\lambda_M|$, which is ignored in our analysis.

A key result is the observation that both K and Γ depend exclusively on a single parameter: λ_X. This highlights the central role λ_X plays in superexchange interactions. We describe the λ_X dependence of K and Γ in Figs. 3(c) and 3(d) using the quadratic relationship revealed in the recent microscopic second-order perturbation theory [27]. Figures 3(f)–3(h) show the magnetocrystalline anisotropy energy $F_c(\theta, \phi)$ for CrX_3 as indicated, where shape anisotropy is excluded. Figure 3(e) shows $F_{c,max} - F_{c,min}$ as a function of $|\lambda_X|$, which mainly reflects the size of uniaxial magnetocrystalline anisotropy energy, where $F_{c,max}$ and $F_{c,min}$ are the maxima and minima of $F_c(\theta, \phi)$. This shows the direct, experimentally obtained relationship between macroscopic magnetic anisotropy and microscopic SOC λ_X arising from the ligand atomic p orbital, which is also well described by a simple quadratic monomial, as is the case for K and Γ.

Crystal structure parameters such as Cr–Cr distance d_{Cr-Cr} in Fig. 1(e) or Cr–X–Cr bond angle $\theta_{Cr-X-Cr}$ in Fig. 1(f) can have a critical effect on K and Γ values as well as J, but none of them shows any noticeable correlation. Recent DFT calculations show that deformation of the monolayer crystal structures of CrX_3 can sensitively influence the magnitude and sign of the exchange interaction parameters [32,35,36]. Indeed, changes in magnetic and electronic properties due to pressure-induced crystal deformation have been observed, such as increases in T_C [37], anomalous magnetoresistance [38], and semiconductor-to-metal transition [38]. In general, superexchange interaction is known to decrease very sensitively, changing by an order of magnitude with sub-Å increases in the spin-spin separation, typically exhibiting an exponential or inverse power-law dependence [39,40]. However, this is not the case for CrX_3, which exhibits the opposite behavior where the magnitudes of J, K, and Γ increase with increasing d_{Cr-Cr} [see Figs. 1(e) and 3(a)]. Also, according to the Goodenough-Kanamori-Anderson rules [41–43], the superexchange interaction is primarily ferromagnetic when $\theta_{Cr-X-Cr}$ is 90°. In this regard, recent DFT calculations for CrX_3 monolayer show that exchange interactions are highly sensitive to small changes in $\theta_{Cr-X-Cr}$ and that the magnetic phase can change from ferromagnetic to antiferromagnetic [36]. However, $\theta_{Cr-X-Cr}$ has no significant X-dependent change around 95.5° and does not show a clear correlation with the spin interaction constant values [see Fig. 1(f)], so its impact appears to be minimal.

Figures 4(a)–4(c) show the spin-wave dispersions for CrX_3 calculated using linear spin-wave theory incorporating J, K, Γ in Fig. 3, and J_2, the NNN Heisenberg interaction. These well describe two magnon bands observed in INS, with the coincident magnon band width $E_{max} - E_{min}$, increasing from $CrCl_3$ [20], through $CrBr_3$ [22], to CrI_3 [5], where E_{max} and E_{max} are the maximum and minimum energies of the magnon band in Figs. 4(a)–4(c). This band width is mainly determined by $|J|$, which also increases in the order of $CrCl_3$, $CrBr_3$, and CrI_3 [see Fig. 3(b)].

The Kitaev interaction plays a major role in opening the Dirac gap Δ_K at the momentum point $\tilde{K}$ [see Fig. 4(d)]. Thus, the size of Δ_K for $|\lambda_X|$ varies roughly in accordance with a quadratic monomial fit, as shown in Fig. 4(g). The first INS reports for $CrBr_3$ and CrI_3 concluded large Δ_K of about 3.5 meV [21] and 5 meV [3], respectively. However, the latest INS, perhaps with reduced sample mosaic and improved instrumental resolution, shows no Dirac gap in $CrCl_3$ [20] and $CrBr_3$ [22], which is more consistent with the results in Fig. 4(g) showing tiny Δ_K for all three CrX_3. DM interaction could be necessary to obtain the correct gap near the Dirac point, not captured by FMR, and not included in the spin-wave plot in Fig. 4. INS suggests a 2.8-meV gap for CrI_3, which is consistent with 0.2-meV DM interaction extracted from DFT [34].

Γ opens a gap Δ_Γ at the zero-momentum point $\tilde{\Gamma}$ that overcomes the Mermin-Wagner theorem by suppressing low-energy magnon excitations, thus enabling 2D long-range ferromagnetic order. The sizes of $\Delta_\Gamma = -3S\Gamma$ for CrX_3 are

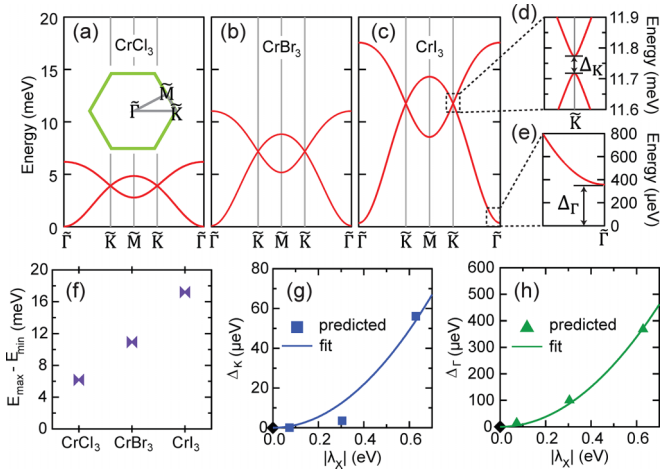

FIG. 4. (a)–(c) Spin-wave dispersions for $CrCl_3$, $CrBr_3$, and CrI_3 predicted from linear spin-wave theory calculations using the measured J, K, and Γ in Fig. 3 and J_2, NNN Heisenberg interaction. (d) Zoom-in showing the Dirac gap Δ_K at $\tilde{K}$. (e) Zoom-in on the region showing the gap Δ_Γ at $\tilde{\Gamma}$. (f) $E_{\max} - E_{\min}$ for CrX_3, where $E_{\max}$ and $E_{\min}$ are the maximum and minimum energies of spin-wave bands in (a)–(c). (g) Δ_K and (h) Δ_Γ values obtained from (a)–(c) for three $|\lambda_X|$ values corresponding to CrX_3 in Fig. 1(d) and their quadratic monomial fits (solid lines) with one more data point (black diamond) added, assuming that Δ_K and Δ_Γ become zero when $\lambda_X = 0$. Note that DM interactions not considered here can lead to larger Δ_K.

shown in Fig. 4(h), where Δ_Γ increases quadratically with increasing $|\lambda_X|$, indicating that it originates from the same ligand SOC as K and $F_{c,\max} - F_{c,\min}$. For CrI_3 we obtain $\Delta_\Gamma = 0.36$ meV, very close to the value 0.37 meV, obtained recently from high-resolution INS [19]. Although not discussed here, single-ion anisotropy $\sim S_z^2$ can also cause uniaxial magnetic anisotropy with the same $\cos^2\theta$ angular dependence of energy as Γ, so its effect is indistinguishable from Γ in field-angle-dependent FMR experiments. However, performing ED calculations using single-ion anisotropy results in a larger gap of 0.61 meV at $\tilde{\Gamma}$, which is somewhat inconsistent with INS. Therefore, it seems the effect of single-ion anisotropy is small and that Γ is the primary source of the observed uniaxial magnetocrystalline anisotropy in Figs. 3(f)–3(h). While Heisenberg and uniaxial anisotropy S_z^2 terms and DM play some roles in governing magnetism in CrI_3, the terms such as $K + \Gamma$ which break the spin conservation perpendicular to the honeycomb plane have been shown to play a crucial role in magneto-optical Kerr effect (MOKE) oscillations, since any dynamics for S_z needs breaking of spin conservation [44].

Interestingly, the size of Δ_K opened by K in Fig. 4(g) is much smaller than the corresponding $|K|$ value in Fig. 3(c), whereas the Δ_Γ value in Fig. 4(h) is much larger than the corresponding $|\Gamma|$ value in Fig. 3(d). This is because the large value of J significantly inhibits K from opening the gap Δ_K, whereas J does not affect the size of Δ_Γ. For example, our calculation for CrI_3 shows that a 50% decrease in $|J|$, while keeping other interaction constants the same, results in a 77% increase in Δ_K.

In conclusion, we present measurements of the spin interaction constants in the $JK\Gamma$ Hamiltonian for three CrX_3 compounds obtained experimentally from field-angle-dependent ferromagnetic resonance and theoretically from exact diagonalization. We find that K and Γ depend dominantly on the ligand SOC λ_X following the quadratic monomial dependence predicted by microscopic second-order perturbation theory. J may suppress the effects of K, such as by inhibiting the opening of the gap Δ_K, which may make it difficult to observe the consequences of the Kitaev interaction, beyond the magnetic anisotropy measured by FMR and reported here. To realize Kitaev physics, studies of J, especially its physical origins and methods of suppressing it, should be conducted in parallel with studies of K. Our experimental discovery of the microscopic mechanism of 2D magnetism in CrX_3 paves the way to design and explore 2D magnetic materials exhibiting novel behaviors by tuning intrinsic material parameters such as spin-orbit coupling.

This research was primarily supported by the Center for Emergent Materials, an NSF MRSEC, under Award No. DMR-2011876. The National High Magnetic Field Laboratory (NHMFL) is funded by the National Science Foundation Division of Materials Research (Grants No. DMR-1644779 and No. DMR-2128556) and the State of Florida. J.C. and H.Y.K. are supported by the NSERC Discovery Grant No. 2022-04601 and the Canada Research Chairs Program No. CRC-2019-00147. This research was enabled in part by support provided by Compute Ontario, Calcul Québec, and the Digital Research Alliance of Canada.

[1] B. Huang, G. Clark, E. Navarro-Moratalla, D. R. Klein, R. Cheng, K. L. Seyler, D. Zhong, E. Schmidgall, M. A. McGuire, D. H. Cobden, W. Yao, D. Xiao, P. Jarillo-Herrero, and X. Xu, Layer-dependent ferromagnetism in a van der Waals crystal down to the monolayer limit, Nature (London) **546**, 270 (2017).

[2] S. A. Owerre, Topological honeycomb magnon Hall effect: A calculation of thermal Hall conductivity of magnetic spin excitations, J. Appl. Phys. **120**, 043903 (2016).

[3] L. Chen, J.-H. Chung, B. Gao, T. Chen, M. B. Stone, A. I. Kolesnikov, Q. Huang, and P. Dai, Topological spin excitations in honeycomb ferromagnet CrI_3, Phys. Rev. X **8**, 041028 (2018).

[4] S. S. Pershoguba, S. Banerjee, J. C. Lashley, J. Park, H. Ågren, G. Aeppli, and A. V. Balatsky, Dirac magnons in honeycomb ferromagnets, Phys. Rev. X **8**, 011010 (2018).

[5] L. Chen, J.-H. Chung, M. B. Stone, A. I. Kolesnikov, B. Winn, V. O. Garlea, D. L. Abernathy, B. Gao, M. Augustin, E. J. G. Santos, and P. Dai, Magnetic field effect on topological spin excitations in CrI_3, Phys. Rev. X **11**, 031047 (2021).

[6] A. Banerjee, C. A. Bridges, J.-Q. Yan, A. A. Aczel, L. Li, M. B. Stone, G. E. Granroth, M. D. Lumsden, Y. Yiu, J. Knolle, S. Bhattacharjee, D. L. Kovrizhin, R. Moessner, D. A. Tennant, D. G. Mandrus, and S. E. Nagler, Proximate Kitaev quantum

spin liquid behavior in a honeycomb magnet, Nat. Mater. **15**, 733 (2016).

[7] K. Kitagawa, T. Takayama, Y. Matsumoto, A. Kato, R. Takano, Y. Kishimoto, S. Bette, R. Dinnebier, G. Jackeli, and H. Takagi, A spin-orbital-entangled quantum liquid on a honeycomb lattice, Nature (London) **554**, 341 (2018).

[8] I. Lee, F. G. Utermohlen, D. Weber, K. Hwang, C. Zhang, J. van Tol, J. E. Goldberger, N. Trivedi, and P. C. Hammel, Fundamental spin interactions underlying the magnetic anisotropy in the Kitaev ferromagnet CrI_3, Phys. Rev. Lett. **124**, 017201 (2020).

[9] C. Xu, J. Feng, M. Kawamura, Y. Yamaji, Y. Nahas, S. Prokhorenko, Y. Qi, H. Xiang, and L. Bellaiche, Possible Kitaev quantum spin liquid state in 2D materials with $S = 3/2$, Phys. Rev. Lett. **124**, 087205 (2020).

[10] A. K. Behera, S. Chowdhury, and S. R. Das, Magnetic skyrmions in atomic thin CrI_3 monolayer, Appl. Phys. Lett. **114**, 232402 (2019).

[11] S. Jiang, J. Shan, and K. F. Mak, Electric-field switching of two-dimensional van der Waals magnets, Nat. Mater. **17**, 406 (2018).

[12] D. R. Klein, D. MacNeill, J. L. Lado, D. Soriano, E. Navarro-Moratalla, K. Watanabe, T. Taniguchi, S. Manni, P. Canfield, J. Fernández-Rossier, and P. Jarillo-Herrero, Probing magnetism in 2D van der Waals crystalline insulators via electron tunneling, Science **360**, 1218 (2018).

[13] J. Cen and H.-Y. Kee, Strategy to extract Kitaev interaction using symmetry in honeycomb Mott insulators, Commun. Phys. **5**, 119 (2022).

[14] J. Cen and H.-Y. Kee, Determining Kitaev interaction in spin-S honeycomb Mott insulators, Phys. Rev. B **107**, 014411 (2023).

[15] Y. Kasahara, T. Ohnishi, Y. Mizukami, O. Tanaka, S. Ma, K. Sugii, N. Kurita, H. Tanaka, J. Nasu, Y. Motome, T. Shibauchi, and Y. Matsuda, Majorana quantization and half-integer thermal quantum Hall effect in a Kitaev spin liquid, Nature (London) **559**, 227 (2018).

[16] T. Yokoi, S. Ma, Y. Kasahara, S. Kasahara, T. Shibauchi, N. Kurita, H. Tanaka, J. Nasu, Y. Motome, C. Hickey, S. Trebst, and Y. Matsuda, Half-integer quantized anomalous thermal Hall effect in the Kitaev material candidate α-$RuCl_3$, Science **373**, 568 (2021).

[17] P. Czajka, T. Gao, M. Hirschberger, P. Lampen-Kelley, A. Banerjee, J. Yan, D. G. Mandrus, S. E. Nagler, and N. P. Ong, Oscillations of the thermal conductivity in the spin-liquid state of α-$RuCl_3$, Nat. Phys. **17**, 915 (2021).

[18] J. A. N. Bruin, R. R. Claus, Y. Matsumoto, N. Kurita, H. Tanaka, and H. Takagi, Robustness of the thermal Hall effect close to half-quantization in α-$RuCl_3$, Nat. Phys. **18**, 401 (2022).

[19] L. Chen, J.-H. Chung, T. Chen, C. Duan, A. Schneidewind, I. Radelytskyi, D. J. Voneshen, R. A. Ewings, M. B. Stone, A. I. Kolesnikov, B. Winn, S. Chi, R. A. Mole, D. H. Yu, B. Gao, and P. Dai, Magnetic anisotropy in ferromagnetic CrI_3, Phys. Rev. B **101**, 134418 (2020).

[20] S.-H. Do, J. A. M. Paddison, G. Sala, T. J. Williams, K. Kaneko, K. Kuwahara, A. F. May, J. Yan, M. A. McGuire, M. B. Stone, M. D. Lumsden, and A. D. Christianson, Gaps in topological magnon spectra: Intrinsic versus extrinsic effects, Phys. Rev. B **106**, L060408 (2022).

[21] Z. Cai, S. Bao, Z.-L. Gu, Y.-P. Gao, Z. Ma, Y. Shangguan, W. Si, Z.-Y. Dong, W. Wang, Y. Wu, D. Lin, J. Wang, K. Ran, S. Li, D. Adroja, X. Xi, S.-L. Yu, X. Wu, J.-X. Li, and J. Wen, Topological magnon insulator spin excitations in the two-dimensional ferromagnet $CrBr_3$, Phys. Rev. B **104**, L020402 (2021).

[22] S. E. Nikitin, B. Fåk, K. W. Krämer, T. Fennell, B. Normand, A. M. Läuchli, and C. Rüegg, Thermal evolution of Dirac magnons in the honeycomb ferromagnet $CrBr_3$, Phys. Rev. Lett. **129**, 127201 (2022).

[23] C. Wellm, J. Zeisner, A. Alfonsov, A. U. B. Wolter, M. Roslova, A. Isaeva, T. Doert, M. Vojta, B. Büchner, and V. Kataev, Signatures of low-energy fractionalized excitations in α-$RuCl_3$ from field-dependent microwave absorption, Phys. Rev. B **98**, 184408 (2018).

[24] A. N. Ponomaryov, L. Zviagina, J. Wosnitza, P. Lampen-Kelley, A. Banerjee, J.-Q. Yan, C. A. Bridges, D. G. Mandrus, S. E. Nagler, and S. A. Zvyagin, Nature of magnetic excitations in the high-field phase of α-$RuCl_3$, Phys. Rev. Lett. **125**, 037202 (2020).

[25] Y. Singh, S. Manni, J. Reuther, T. Berlijn, R. Thomale, W. Ku, S. Trebst, and P. Gegenwart, Relevance of the Heisenberg-Kitaev model for the honeycomb lattice iridates A_2IrO_3, Phys. Rev. Lett. **108**, 127203 (2012).

[26] H. Gretarsson, J. P. Clancy, X. Liu, J. P. Hill, E. Bozin, Y. Singh, S. Manni, P. Gegenwart, J. Kim, A. H. Said, D. Casa, T. Gog, M. H. Upton, H.-S. Kim, J. Yu, V. M. Katukuri, L. Hozoi, J. van den Brink, and Y.-J. Kim, Crystal-field splitting and correlation effect on the electronic structure of A_2IrO_3, Phys. Rev. Lett. **110**, 076402 (2013).

[27] P. P. Stavropoulos, X. Liu, and H.-Y. Kee, Magnetic anisotropy in spin-3/2 with heavy ligand in honeycomb Mott insulators: Application to CrI_3, Phys. Rev. Res. **3**, 013216 (2021).

[28] C. E. Moore, *Atomic Energy Levels: As Derived from the Analyses of Optical Spectra* (US Department of Commerce, National Bureau of Standards, Washington, DC, 1971).

[29] J. L. Lado and J. Fernández-Rossier, On the origin of magnetic anisotropy in two dimensional CrI_3, 2D Mater. **4**, 035002 (2017).

[30] D.-H. Kim, K. Kim, K.-T. Ko, J. H. Seo, J. S. Kim, T.-H. Jang, Y. Kim, J.-Y. Kim, S.-W. Cheong, and J.-H. Park, Giant magnetic anisotropy induced by ligand *LS* coupling in layered Cr compounds, Phys. Rev. Lett. **122**, 207201 (2019).

[31] M. McGuire, Crystal and magnetic structures in layered, transition metal dihalides and trihalides, Crystals **7**, 121 (2017).

[32] L. Webster and J.-A. Yan, Strain-tunable magnetic anisotropy in monolayer $CrCl_3$, $CrBr_3$, and CrI_3, Phys. Rev. B **98**, 144411 (2018).

[33] See Supplemental Material at http://link.aps.org/supplemental/10.1103/qg64-ztxj for detailed information on samples, experiments, theoretical calculations, and additional data, which includes Refs. [45,46].

[34] S. Bandyopadhyay, F. L. Buessen, R. Das, F. G. Utermohlen, N. Trivedi, A. Paramekanti, and I. Dasgupta, Exchange interactions and spin dynamics in the layered honeycomb ferromagnet CrI_3, Phys. Rev. B **105**, 184430 (2022).

[35] Z. Wu, J. Yu, and S. Yuan, Strain-tunable magnetic and electronic properties of monolayer CrI_3, Phys. Chem. Chem. Phys. **21**, 7750 (2019).

[36] M. Pizzochero and O. V. Yazyev, Inducing magnetic phase transitions in monolayer CrI_3 via lattice deformations, J. Phys. Chem. C **124**, 7585 (2020).

[37] S. Mondal, M. Kannan, M. Das, L. Govindaraj, R. Singha, B. Satpati, S. Arumugam, and P. Mandal, Effect of hydrostatic

pressure on ferromagnetism in two-dimensional CrI_3, Phys. Rev. B **99**, 180407(R) (2019).

[38] A. Ghosh, D. Singh, T. Aramaki, Q. Mu, V. Borisov, Y. Kvashnin, G. Haider, M. Jonak, D. Chareev, S. A. Medvedev, R. Klingeler, M. Mito, E. H. Abdul-Hafidh, J. Vejpravova, M. Kalbàč, R. Ahuja, O. Eriksson, and M. Abdel-Hafiez, Exotic magnetic and electronic properties of layered CrI_3 single crystals under high pressure, Phys. Rev. B **105**, L081104 (2022).

[39] R. E. Coffman and G. R. Buettner, A limit function for long-range ferromagnetic and antiferromagnetic superexchange, J. Phys. Chem. **83**, 2387 (1979).

[40] S. K. Hoffmann, W. Hilczer, and J. Goslar, Weak long-distance superexchange interaction and its temperature variations in copper(II) compounds studied by single crystal EPR, Appl. Magn. Reson. **7**, 289 (1994).

[41] J. B. Goodenough, An interpretation of the magnetic properties of the perovskite-type mixed crystals $La_{1-x}Sr_xCoO_{3-\lambda}$, J. Phys. Chem. Solids **6**, 287 (1958).

[42] J. Kanamori, Superexchange interaction and symmetry properties of electron orbitals, J. Phys. Chem. Solids **10**, 87 (1959).

[43] P. W. Anderson, New approach to the theory of superexchange interactions, Phys. Rev. **115**, 2 (1959).

[44] P. Padmanabhan, F. L. Buessen, R. Tutchton, K. W. C. Kwock, S. Gilinsky, M. C. Lee, M. A. McGuire, S. R. Singamaneni, D. A. Yarotski, A. Paramekanti, J.-X. Zhu, and R. P. Prasankumar, Coherent helicity-dependent spin-phonon oscillations in the ferromagnetic van der Waals crystal CrI_3, Nat. Commun. **13**, 4473 (2022).

[45] J. van Tol, L.-C. Brunel, and R. J. Wylde, A quasioptical transient electron spin resonance spectrometer operating at 120 and 240 GHz, Rev. Sci. Instrum. **76**, 074101 (2005).

[46] G. M. Smith, J. C. G. Lesurf, R. H. Mitchell, and P. C. Riedi, Quasi-optical cw mm-wave electron spin resonance spectrometer, Rev. Sci. Instrum. **69**, 3924 (1998).